Lipid Emulsion–Based OCT Angiography for Ex Vivo Imaging of the Aqueous Outflow Tract

Hanna M. Gottschalk,[1] Thomas Wecker,[2] Mohammed H. Khattab,[1] Charlotte V. Fischer,[1] Josep Callizo,[1] Florian Rehfeldt,[3] Roswitha Lubjuhn,[4] Christoph Russmann,[5,6] Hans Hoerauf,[1] and Christian van Oterendorp[1]

[1]Department of Ophthalmology, University Medical Center, Göttingen, Germany
[2]Ophthalmic practice Dr. Wecker, Heilbronn, Germany
[3]Third Institute of Physics, Biophysics, Georg-August-University, Göttingen, Germany
[4]Department of Anaesthesiology, University Medical Center, Göttingen, Germany
[5]Faculty of Natural Science and Technology, University of Applied Sciences and Arts, Göttingen, Germany
[6]Molecular Biomarkers Nano-Imaging Laboratory, Brigham and Women's Hospital, and Department of Radiology, Harvard Medical School, Boston, Massachusetts, United States

PURPOSE. Contrast agents applicable for optical coherence tomography (OCT) imaging are rare. The intrascleral aqueous drainage system would be a potential application for a contrast agent, because the aqueous veins are of small diameter and located deep inside the highly scattering sclera. We tested lipid emulsions (LEs) as candidate OCT contrast agents in vitro and ex vivo, including milk and the anesthetic substance Propofol.

METHODS. Commercial OCT and OCT angiography (OCTA) devices were used. Maximum reflectivity and signal transmission of LE were determined in tube phantoms. Absorption spectra and light scattering was analyzed. The anterior chamber of enucleated porcine eyes was perfused with LEs, and OCTA imaging of the LEs drained via the aqueous outflow tract was performed.

RESULTS. All LEs showed a significantly higher reflectivity than water ($P < 0.001$). Higher milk lipid content was positively correlated with maximum reflectivity and negatively with signal transmission. Propofol exhibited the best overall performance. Due to a high degree of signal fluctuation, OCTA could be applied for detection of LE. Compared with blood, the OCTA signal of Propofol was significantly stronger ($P = 0.001$). As a proof of concept, time-resolved aqueous angiography of porcine eyes was performed. The three-dimensional (3D) structure and dynamics of the aqueous outflow were significantly different from humans.

CONCLUSIONS. LEs induced a strong signal in OCT and OCTA. LE-based OCTA allowed the ability to obtain time-resolved 3D datasets of aqueous outflow. Possible interactions of LE with inner eye's structures need to be further investigated before in vivo application.

Keywords: optical coherence tomography angiography, aqueous flow, lipid emulsion, propofol

The intrascleral aqueous drainage system comprising of collector channels and aqueous veins still remains one of the most poorly characterized structures in the eye. Its complex network of small vessels lying deep in the highly scattering sclera[1,2] is difficult to resolve in morphologic optical coherence tomography (OCT) imaging.[3,4] Moreover, due to the monophasic nature of the aqueous humor, OCT angiography (OCTA) is not directly applicable to detect aqueous humor flow. The current advent of glaucoma surgical techniques targeting the trabecular meshwork has increased the need to expand our fragmentary knowledge of structure and function of the aqueous drainage system.[5,6] Recently, fluorescent dyes, such as fluorescein and indocyanine green (ICG), have been successfully used for aqueous angiography in animals and human.[7,8] However, this approach is limited to two-dimensional (2D) images of the target structures.

OCT has become a major diagnostic and research tool in ophthalmology.[9,10] Spectral domain (SD)-OCT is the current standard technology, using superluminescent diode light sources with a spectral bandwidth centered approximately 840 to 880 nm in the commercial devices for clinical application.[11] Their scanning speed is limited mainly by the processing speed of their spectral sensor. In contrast, swept source (SS)-OCT is an emerging technology enabling significantly higher A-scan rates.[12,13] Utilization of longer wavelengths decreases signal loss due to scattering and thus increases tissue penetration of the scanning beam.[10]

Recently, OCTA has been introduced as a novel clinical imaging modality. Its image processing algorithms allow for specific detection of highly fluctuating signals derived, for example, from flowing blood inside blood vessels.[14,15]

Unlike other imaging modalities in medicine, OCT lacks an established contrast agent. Gold nanorods have been successfully used under experimental conditions.[16–18] However, they are relatively expensive, and toxicity or other side effects of their application remain to be investigated.[19,20] Lipid emulsions

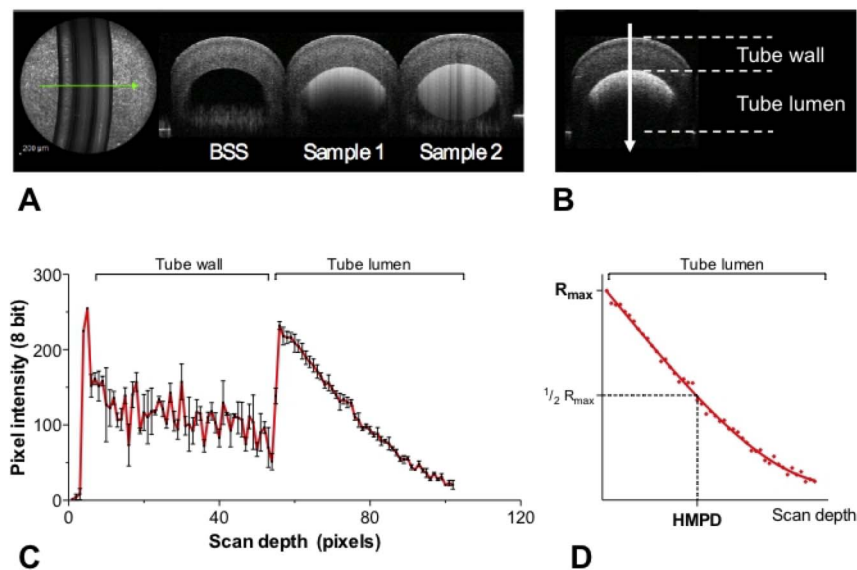Investigative Ophthalmology & Visual Science

FIGURE 1. Imaging phantoms and principle of OCT intensity plots. (A) Original scan image as exported from the SD-OCT. *Left:* SLO image of the phantom, consisting of three polyethylene tubes, mounted on black cardboard. One of the three tubes was always filled with BSS to provide a reference for brightness normalization. The *green line* indicates the position of the OCT scan. *Right:* OCT B-scan (30 frames averaged; image cropped to the phantom). (B) Indication of the intensity plot position and direction (*white arrow*). (C) Complete intensity plot including the polyethylene tube wall and lumen filled with the candidate substances. The *red line* connects the mean of three measurements at different locations. *Error bars* indicate SD. (D) Illustration of R_{max} and HMPD measurement. Only the plot inside the tube lumen was used, and a fourth-order polynomial function was fitted before determination of R_{max} and HMPD.

(LEs) are known to produce an OCT signal shift relative to water (van Oterendorp C, et al. *IOVS* 2016;57:ARVO E-Abstract 474). LE eye drops have been used to improve the visibility of the tear meniscus in anterior segment OCT imaging.[21] A soybean oil–based LE (Intralipid; Sigma-Aldrich Chemie GmbH, Munich, Germany) has recently been used to enhance contrast and to measure flow velocities in optical Doppler tomography–based imaging of mouse brain capillary networks.[22] However, there are no published studies comparing different LEs regarding their effectiveness as contrast agents in various OCT setups.

In this in vitro and ex vivo study, we investigated the optical properties of different LEs (milk and Propofol) and applied them to commercial OCT and OCTA setups. As a proof of concept, we used LE-based OCTA to demonstrate the feasibility of this approach for time-resolved 3D imaging of the aqueous outflow tract in ex vivo pork eyes.

METHODS

OCT Devices and Liquids Used

OCT images were acquired with standard clinical diagnostic OCT devices. Either an SD-OCT (Spectralis OCT with anterior segment module; Heidelberg Engineering, Heidelberg, Germany) with a light spectrum centered around 870 nm or an SS-OCT (SS-1000; Tomey GmbH, Erlangen, Germany) with a maximum wavelength of 1300 nm was used. For OCTA imaging, a Zeiss Cirrus Angioplex device (Carl Zeiss Meditec, Jena, Germany) equipped with an OCTA anterior segment imaging module was used. This imaging module was a prototype provided from Carl Zeiss Meditech (Dublin, CA, USA).

The LEs used were either different types of milk (semi-skimmed [1.5%], full fat [3.8%], and coffee cream [12%]) or 1% Propofol (Propofol-Lipuro 10 mg/mL; B. Braun Melsungen AG,

Melsungen, Germany). Balanced salt solution (BSS) was used as monophasic control liquid.

Phantom Imaging

An imaging phantom, built from three polyethylene test tubes with 1-mm inner and 2-mm outer diameter (Injectomat line; Fresenius-Kabi, Bad-Homburg, Germany), was filled with different liquid samples and mounted in front of the OCT device (Fig. 1A). B-scan cross sections of the phantom were obtained (Fig. 1B). During the scan, no flow was induced in the tubes. Either not averaged B-scans or averaged scans (SD-OCT only), using the built-in image averaging algorithms (automatic real-time averaging; Heidelberg Engineering) set to 30 B-scans per section, were obtained.

Phantom Image Processing and Analysis

Images were exported in TIFF format and further processed and analyzed with ImageJ/FIJI software.[23] First, images were transformed from RGB to eight-bit grayscale. To correct for differences in global image brightness between different scans, normalization was performed, using the signal intensity inside the polyethylene wall of a BSS-filled control tube as reference. For this reason, a BSS control tube was included in every scan.

For quantification of the reflectivity signal, pixel intensity plots along the A-scan axis (arrow in Fig. 1B) were obtained from averaged B-scans as illustrated in Figure 1C. For SD-OCT scans, the built-in automatic averaging functionality was used (30 frames averaging per scan). For SS-OCT scans, a stack of 30 consecutive B-scans from the same location was first registered (rigid body) and then averaged using ImageJ/FIJI's Stackreg and Z projection tool.

Different intensity plots per liquid sample ($n = 3$) were collected from different locations near the central axis of the tube. The central axis itself was avoided due to a reflection of the tube surface, potentially interfering with the intensity measurement.

The properties of the sample liquids were compared regarding two parameters (Fig. 1D): (1) maximum reflectivity derived from the substance in the tube lumen, termed R_{max} and (2) the intraluminal scan depth at which $\frac{1}{2}R_{max}$ was reached, as a measure of the signal decay inside the liquid, termed HMPD (half maximum penetration depth). To determine HMPD, a fourth-order polynomial function was fitted to $n = 3$ normalized intensity plots using GraphPad Prism V6.0 software (GraphPad, La Jolla, CA, USA). The fourth-order polynomial function was chosen as an approximation to the logarithmic attenuation of light following Beer-Lambert's law. From this function, HMPD (in pixel) was calculated.

For calculation of signal fluctuation over time, a series of 12 consecutive unaveraged B-scans was acquired with the SD-OCT, using a noncommercial feature of the Spectralis OCT device software. The images were exported in TIFF format and further processed with ImageJ/FIJI. After eight-bit gray scale conversion and registration, a Z-projection of the image stack was performed, calculating either the average pixel intensity or the SD of pixel intensity as a measure of signal fluctuation. In the latter images, a line triplet (each line 30 pixels) was placed inside each sample or, for reference purposes, inside a BSS-tube wall. The pixel intensity of the resulting 90 pixels per sample was compared. The resulting pixel intensity values represent the signal fluctuation over time.

Spectroscopy

Samples of milk (1.5%, 3.8%, and 12% fat) and Propofol were diluted 1:10 with PBS and analyzed in a spectrophotometer (PharmaSpec UV-1700; Shimadzu, Tokyo, Japan). Absorption (including scattering) was quantified in direct transmission geometry within a spectral range of 400 to 1100 nm (maximum wavelength of the instrument).

Dynamic Light Scattering

Samples of milk (1.5%, 3.8%, and 12% fat) and Propofol were diluted 1:100 with degassed PBS. Dynamic light scattering (DLS) measurements were performed on an ALV/CGS-3 Laser Light Scattering Goniometer System (ALV GmbH, Langen, Germany) at a wavelength of 632 nm (HeNe laser #1145P; JDS Uniphase, Milpitas, CA, USA). Scattered photons were recorded under an angle of 90° with respect to the optical axis.

Data were analyzed with the Sedfit software[24] using the cumulant analysis algorithm.

Ex Vivo Imaging

Enucleated porcine eyes obtained from a local abattoir were used. For OCT scanning, the eyes were placed in a custom-made funnel, applying slight suction to the posterior pole for holding the eye in place. The anterior chamber was cannulated to perfuse the eye with either BSS or an LE. The height of the liquid infusion system was set to provide approximately 10 mm Hg IOP (13 to 15 cm water level). By choosing a relatively low infusion pressure, we took into account that no episcleral venous pressure was present in our model. The porcine eyes eye pressure has been reported to be approximately 15 mm Hg,[25] but no data on the episcleral venous pressure were available. We thus set a relatively low perfusion pressure to avoid an unphysiologic pressure gradient and the occurrence of perfusion artifacts.

For OCTA imaging, perfusion of the anterior chamber was performed with either undiluted or diluted (25%, 50%) 10 mg/mL Propofol solution, using PBS as diluent. Either 6- × 6- or 3- × 3-mm scans were obtained approximately every 30 seconds in the early phase of perfusion and at larger time intervals (up to 3 minutes) at later phases. En face images were exported from the device software with the layer segmentation manually set to maximum values (no layer segmentation). In addition, the whole volumetric dataset was exported to present B-scan images. Extraction of substacks, brightness adjustment, noise reduction (remove outliers plugin), reslicing of the stack, and maximum intensity projection calculation were performed with ImageJ/FIJI software.

The scan time was measured as time between start of acquisition and the time point where the device was ready for the next acquisition.

Scanning laser ophthalmoscope (SLO) imaging with ICG as a contrast agent was performed with a commercial device for clinical use (Heidelberg retina angiograph; Heidelberg Engineering) with a 30° retina lens. Five milligrams per milliliter ICG solution (Verdye, Diagnostic Green GmbH, Aschheim-Dornach, Germany) was used to perfuse the anterior chamber. Nine images per region were averaged to improve signal-to-noise ratio.

Histology of the Intrascleral Aqueous Drainage System

Ex vivo procine eyes were perfused through the anterior chamber with 0.4% trypan blue solution (Sigma-Aldrich, St. Louis, MO, USA). Corneo-scleral wedges, containing the chamber angle, were cut out, embedded in glycerin-based Tissue-Tek O.C.T. Compound (Sakura Finetek, Alphen aan den Rijn, Netherlands), snap frozen, and kryosectioned (18 μm thickness). All consecutive sections were collected on super-frost slides (Menzel-Gläser SUPERFROST, ThermoFisher Scientific, Braunschweig, Germany) and photographed on a white surface in reflected light mode with a Leica S6D stereomicroscope and a Leica DFC420 C camera (Leica Microsystems GmbH, Wetzlar, Germany). Images were globally adjusted for contrast and brightness using ImageJ/FIJI. The trypan blue signal was extracted by splitting the RGB channels and subtracting the blue from red channel using the Image calculator plugin. A stack of 23 consecutive trypan blue images was brightness-normalized and registered using the SIFT registration plugin. Noise was reduced by 3D median filtering (2-pixel width), and the stack was rendered in 3D using the Volume viewer plugin.

Statistical Testing

Data plotting and statistical testing were performed with Prism V6.0 software (GraphPad). For comparison between different samples, ANOVA with Sidak's multiple comparison test was performed. Data are presented as mean ± SEM if not stated differently.

RESULTS

Maximum Reflectivity and Penetration Depth of Different LEs in Tube Phantoms

All LEs showed a significantly higher maximum reflectivity (R_{max}) than BSS, which produced no signal above noise (Figs. 2D, 2H). When using different types of milk and cream, ranging from 1.5% to 12% fat, a higher fat content was associated with an increase in R_{max}. This applied to both SD- and SS-OCT devices using a light source of 870 (center wavelength) and 1300 nm (maximum wavelength), respectively (Figs. 2A–2H; Table). At the same time, higher fat content significantly reduced the transmission of light, as indicated by lower HMPD values (milk 1.5% versus milk 12%: $P < 0.0001$ for R_{max} and HMPD with SD- and SS-OCT; $n = 3$). The longer wavelength of
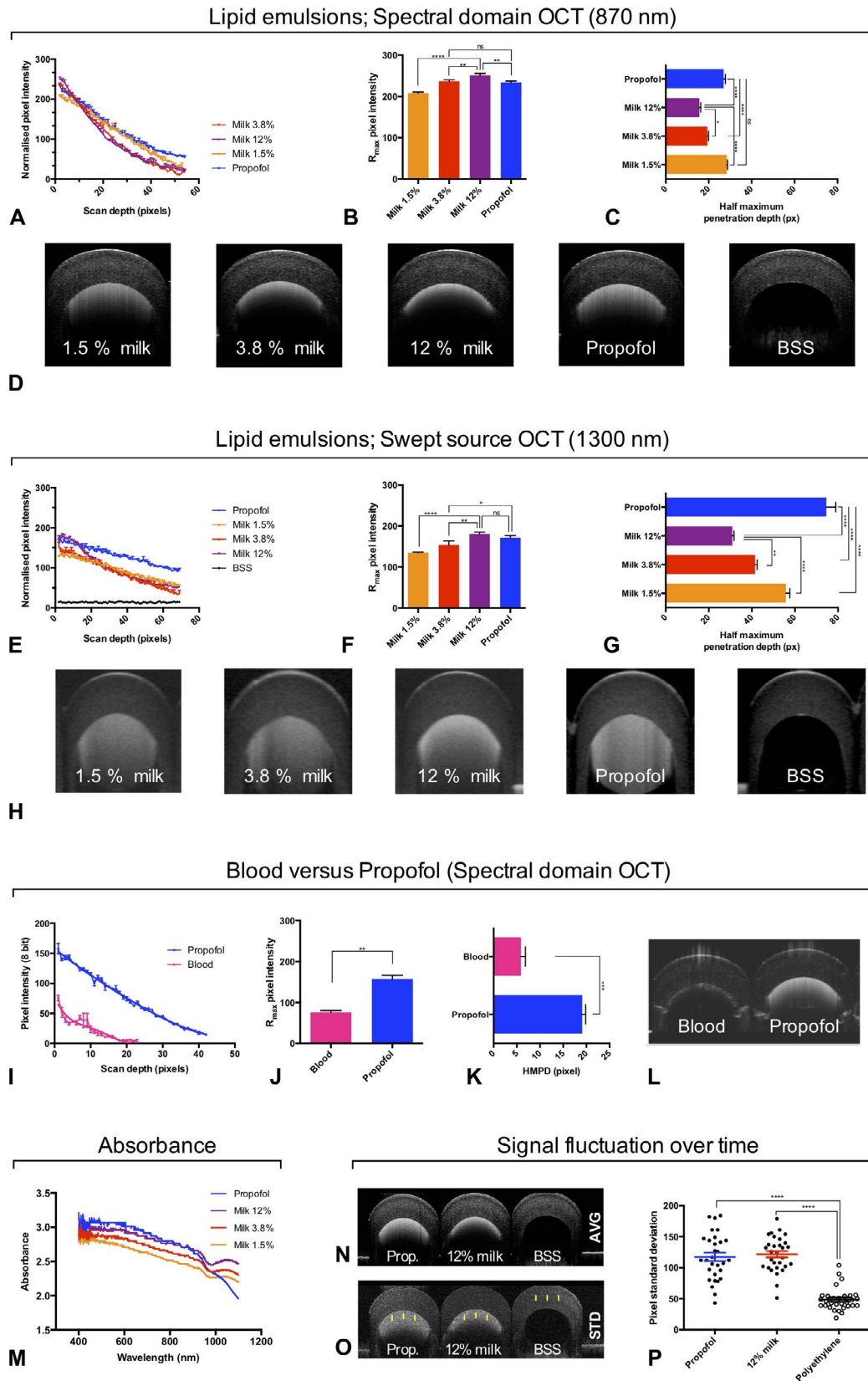
FIGURE 2. In vitro properties of different LEs. (**A–H**) Quantification of maximum reflectivity and penetration depth (R_{max} and HMPD) of different LEs with two different OCT devices (SD-OCT (870 nm) and SS-OCT (1300 nm)). Normalized pixel intensity plots of each LE (**A**, **E**), R_{max} (**B**, **F**), and HMPD (**C**, **G**) were obtained. The *bottom row* in each segment (**D**, **H**) shows representative OCT scans from which the quantification data was obtained. Higher milk fat content was associated with higher R_{max} and lower HMPD. However, Propofol exhibited high values in both measures. (**I**–**L**) Comparison of blood and Propofol. Intensity plot (**I**), R_{max} (**J**), and HMPD (**K**) show significantly higher values for Propofol (R_{max}, $P = 0.0012$; HMPD, $P = 0.0004$). (**L**) Representative OCT images. (**M**) Spectroscopy of milk and Propofol samples. Absorption (partially containing scattering)

was measured from 400 to 1100 nm (the maximum wavelength of the instrument) and is displayed as absorbance versus the wavelength. At 1060 nm, all milk samples but not Propofol exhibited an slight increase in absorbance. (N–P) Quantification of temporal signal fluctuation. Averaged (N) or SD (O) images were calculated from 12 nonaveraged OCT scans. (P) Comparison of the SD between Propofol, 12% milk, and the solid phase phantom tube (baseline noise). Thirty pixels were measured per sample along the *yellow lines*. Both samples exhibited significantly higher signal fluctuation than the baseline noise ($P < 0.0001$). There was no significant difference between the samples ($P = 0.8$). Note the backward projection of the Propofol signal fluctuation into the tube wall in (O).

the SS-OCT resulted in a better overall transmission (higher HMPD) compared with SD-OCT (Figs. 2A–2H; Table).

Propofol, an anesthetic LE, was also tested. R_{max} inside the test tubes was slightly, but significantly lower, compared with 12% milk in SD-OCT scans ($P = 0.002$; Fig. 2B). In the SS-OCT scans, the difference was not significant ($P = 0.27$; Fig. 2F). However, the light transmission (HMPD) of Propofol was higher than 12% milk in SD-OCT and much higher than any milk sample in SS-OCT ($P < 0.0001$ for both devices; Figs. 2C, 2G; Table).

To set the properties of the LEs into relation with a known reference substance, we compared Propofol with blood, which, in OCTA, has been established as a quasi "natural" in vivo contrast agent. Comparative phantom scans of blood and Propofol demonstrated a significantly higher maximum reflectivity and signal transmission of Propofol compared with blood (Figs. 2I–2L; blood versus Propofol: R_{max}: 76 ± 4.6 vs. 158 ± 8.8; $P = 0.0012$, *t*-test; HMPD: 5.9 ± 1.0 vs. 19.1 ± 0.7, $P = 0.0004$, *t*-test; $n = 3$).

Light Absorption and Scattering Characteristics of LEs

To analyze the relative increase of light transmission in Propofol compared with milk at higher wavelengths, absorption spectroscopy was performed for all LEs. All milk samples

revealed a relative increase in absorption toward high wavelengths (950 to 1100 nm), whereas Propofol showed a significant decrease in absorption in the same range (Fig. 2M). Thus, we concluded that significant absorption of light occurred in milk when scanning with long wavelengths, whereas, in Propofol, light transmission was mainly determined by scatter.

To further investigate the light interaction characteristics of the LEs, DLS measurements were performed. Based on a cumulant model, the analysis showed a positive correlation between the particle size and the fat content of the milk samples. The hydrodynamic radius of the lipid aggregates ranged from 150.0 ±1.3 nm for 1.5% milk to 227.9 ± 5.4 nm for 12% milk, whereas Propofol consisted of smaller aggregates with a radius of only 107.6 ± 2.7 nm. DLS also revealed the rather monodisperse character of Propofol (polydispersity index, 0.20) in contrast to the milk samples (polydispersity indices between 0.34 and 0.39).

High Temporal Fluctuation of the OCT Signal from LEs

Besides high reflectivity, a strong and high-frequency temporal fluctuation of the OCT signal was observed with all LEs. This fluctuation occurred in the absence of flow inside the tube phantom. To specifically quantify the signal fluctuation, a time sequence of 12 unprocessed B-scans was obtained from the SD-OCT device, and the pixel SD (PSD) over time was calculated, producing SD images (Figs. 2N–2P). To obtain the basic noise of the OCT device, we quantified the PSD within the wall of a BSS-filled polyethylene tube (indicated in Fig. 2O), presuming that the solid phase of the polyethylene material did not induce a signal fluctuation. Then the PSD was obtained from a 12% milk and Propofol sample inside the tube lumen. In both samples, the mean PSD was significantly higher than the baseline noise measured in the polyethylene tube wall (Fig. 2P; Propofol: 118 ± 6.8; 12% milk: 121 ± 5.2; polyethylene: 49 ± 3.3; $n = 30$ pixels; $P < 0.0001$ for Propofol and milk versus polyethylene). The difference between Propofol and 12% milk was not significant ($P = 0.83$).

Application of OCTA for LE-Based Aqueous Angiography

The high temporal fluctuation of the LE-derived OCT signal allowed us to use OCTA technology. We used this approach to

FIGURE 3. Experimental setup for ex vivo porcine eye scans. The OCT device was equipped with an add-on lens (1). The eyeball (*asterisk*) was placed in a custom-made funnel (2). Slight suction from a pipetting ball (3) kept the eye attached. The eye's anterior chamber was perfused through an open infusion system (4).

TABLE. Maximum Reflectivity (Eight-Bit Gray Values) and HMPD (Number of Pixels) of Different LEs Detected With SD- and SS-OCT

Lipid Emulsion	SD-OCT		SS-OCT	
	R_{max}	HMPD	R_{max}	HMPD
1.5% milk	207 ± 1.8	28 ± 0.2	135 ± 0.9	56 ± 1.1
3.8% milk	237 ± 1.8	19 ± 0.3	154 ± 5.6	41 ± 0.6
12% milk	251 ± 2.9	16 ± 0.4	181 ± 2.4	31 ± 0.4
Propofol	234 ± 2.0	27 ± 0.5	171 ± 3.2	75 ± 2.5

Intensity values were only normalized between the samples scanned with one device but not between the ones with two devices. Thus, the values of SD- and SS-OCT cannot be directly compared.

demonstrate, as a proof of concept, the feasibility of LE-based OCTA for aqueous angiography. Based on the above-described in vitro testing of different LEs, Propofol was chosen as the best performing contrast agent.

Ex vivo porcine eyes were mounted in front of a commercial OCTA device, equipped with a prototype anterior segment OCTA module (Fig. 3). Roughly one quadrant of the eye's circumference could thus be scanned. Time-resolved OCTA imaging (Figs. 4A–4L) revealed that the aqueous was primarily drained via a small number (presumably less than one per quadrant) of large aqueous veins, arising from the chamber angle. These veins presumably represent the angular aqueous plexus, described by McMenamin and Steptoe.[26] They either branched into two large veins or the one vein just bent to run in a limbus-parallel direction. From those large radial and limbus-parallel veins, a fine juxtalimbal network of branches arose (Figs. 4A–4D). It was mainly located anterior to the large limbus-parallel vein. However, despite its proximity to the anterior chamber, it has never been directly perfused from it (Figs. 4A–4D). The drainage of aqueous to the episcleral veins occurred directly from primary aqueous veins. Therefore, in contrast to the human eye, the aqueous is primarily collected by a small number of large diameter aqueous veins, from which it takes two ways, either direct drainage to the episcleral veins or distribution to a fine juxtalimbal intrascleral aqueous vein plexus. The time between start of perfusion and complete filling of all aqueous veins was approximately 5 to 6 minutes at 10 mm Hg perfusion pressure (Fig. 4D).

In addition to the en face images, overlaid OCT/OCTA B-scans revealed that all aqueous veins were found at one single superficial level in the sclera (Figs. 4E–4L and 4Q–4X), which is in contrast to the human eye, where a deep and a superficial vein plexus exists. The fine juxtalimbal plexus of vein branches arising from the primary veins was not connected to the anterior chamber. Instead it seemed to dead end above the chamber angle (Figs. 4D, 4L, 4M–4P, 4U–4X). It remained unclear whether the aqueous reaching this plexus was further drained somewhere. Histologic sections from eyes perfused with Trypan blue instead of Propofol confirmed the presence of only one superficial aqueous plexus and the presence of few, large diameter primary aqueous veins, draining directly from the chamber angle (Fig. 4Y1–3).

The biphasic nature of LE contrast agents raised the question of whether the aqueous flow pattern described above could be aberrant due to obstruction of small vessels by LE droplets. Consequently, the pattern would be different when using monophasic water-based substances, such as ICG. Thus, ICG aqueous angiography was performed using the same setup for perfusion of the anterior chamber. It revealed the same pattern of filling and aqueous distribution as the LE (Supplementary Fig. S1). The speed of contrast agent distribution appeared, at comparable perfusion pressure, not significantly different to LEs. No aqueous vessels smaller than the ones detected with LE OCTA were found. Thus, we concluded that in porcine eyes, the main aqueous drainage structures are the small number of primary aqueous veins arising directly from the anterior chamber. The functional role of the juxtalimbal intrascleral aqueous vein plexus remained unclear.

A further increase in signal-to-noise ratio was achieved by averaging OCTA en face images, as well as B-scans. Figure 5 shows representative scans from two different eyes, comparing conventional "single take" scans and four image average scans. The minimum acquisition time for each single scan was 18 seconds (i.e., the time from starting image acquisition until the device was ready for the next acquisition). Thus, taking four consecutive scans for averaging took minimum 72 seconds. For this reason, averaging was not applied at the early perfusion phase of LE but only at the later steady-state perfusion phase (>5 minutes from start of perfusion).

DISCUSSION

This study demonstrated that LEs exhibit specific features, which qualify them as contrast agents for OCT imaging. These are (1) a high reflectivity and (2) a high level of signal fluctuation. The latter allows the use of OCTA technology for direct detection of the contrast agent. This has been applied, in a proof-of-concept approach, for LE-based aqueous angiography in ex vivo porcine eyes.

When assessing the optical properties of different LEs, Propofol had the best overall performance of high reflectivity, good penetration depth, and low absorption. Moreover, Propofol is approved for in vivo application in humans and thus complies with high standards regarding sterility, non-toxicity, and homogeneity of the emulsion. This might be particularly important for potential in vivo application in animals. As the Propofol molecule itself is presumably of no importance for the optical properties of the LE, a comparable drug-free carrier emulsion, such as Intralipid (Sigma-Aldrich), could have been used instead. The reason for us to use Propofol was its availability in the hospital. In cases where medical grade LEs are either not available or not needed, milk could be a low-cost alternative.

Besides the fact that the drug-free carrier solution would probably be the safer choice for a potential future human application, we believe that even Propofol would not be harmful to the patient with regard to its narcotic properties. Given the use of a 50% diluted solution, the amount of pure Propofol applied for one perfusion would be less than 1 mL (=10 mg Propofol). From this single dose, a mild antiemetic but no narcotic effect would be expected. In principle, repeated use might promote psychologic dependence, but no physical dependence has been described for Propofol. After uptake to the human body, Propofol has an elimination half-life of approximately 60 minutes, and its sedating effect (if sufficiently dosed) lasts for 5 to 8 minutes. Thus, it has the highest plasma clearance of all narcotic substances. After hepatic conjugation and glucuronidation, the substance is eliminated renally. Most importantly, by using the drug-free carrier solution instead of Propofol, researchers could circumvent any problems related to handling a potentially addictive substance.

In the ex vivo application, a dilution of Propofol to 50% led to no visible decrease in OCTA signal strength. Further dilution to 25% resulted in a slightly weaker signal but was still well usable.

Other than LEs, gold nanorods are already well characterized for different imaging modalities, including OCT under experimental conditions. Through coupling to antibodies or chemical compounds, they provide excellent potential for targeted labeling of cell populations and may thus prove particularly useful for molecular biology–based diagnosis of diseases. Besides being relatively expensive, cellular uptake and toxic effects may occur. If the aim is just to produce contrast within defined hollow structures, such as aqueous veins, LEs may prove an affordable and easier to handle alternative.

In our aqueous angiography approach, no apparent deviation from the pattern observed with ICG-based aqueous angiography was seen. Therefore, at least in this ex vivo setup, clogging of small vessels by lipid droplets has not been a problem. Given the DLS-derived hydrodynamic radius of approximately 100 nm, Propofol lipid droplets were much smaller than the vessel diameter of the angular aqueous plexus
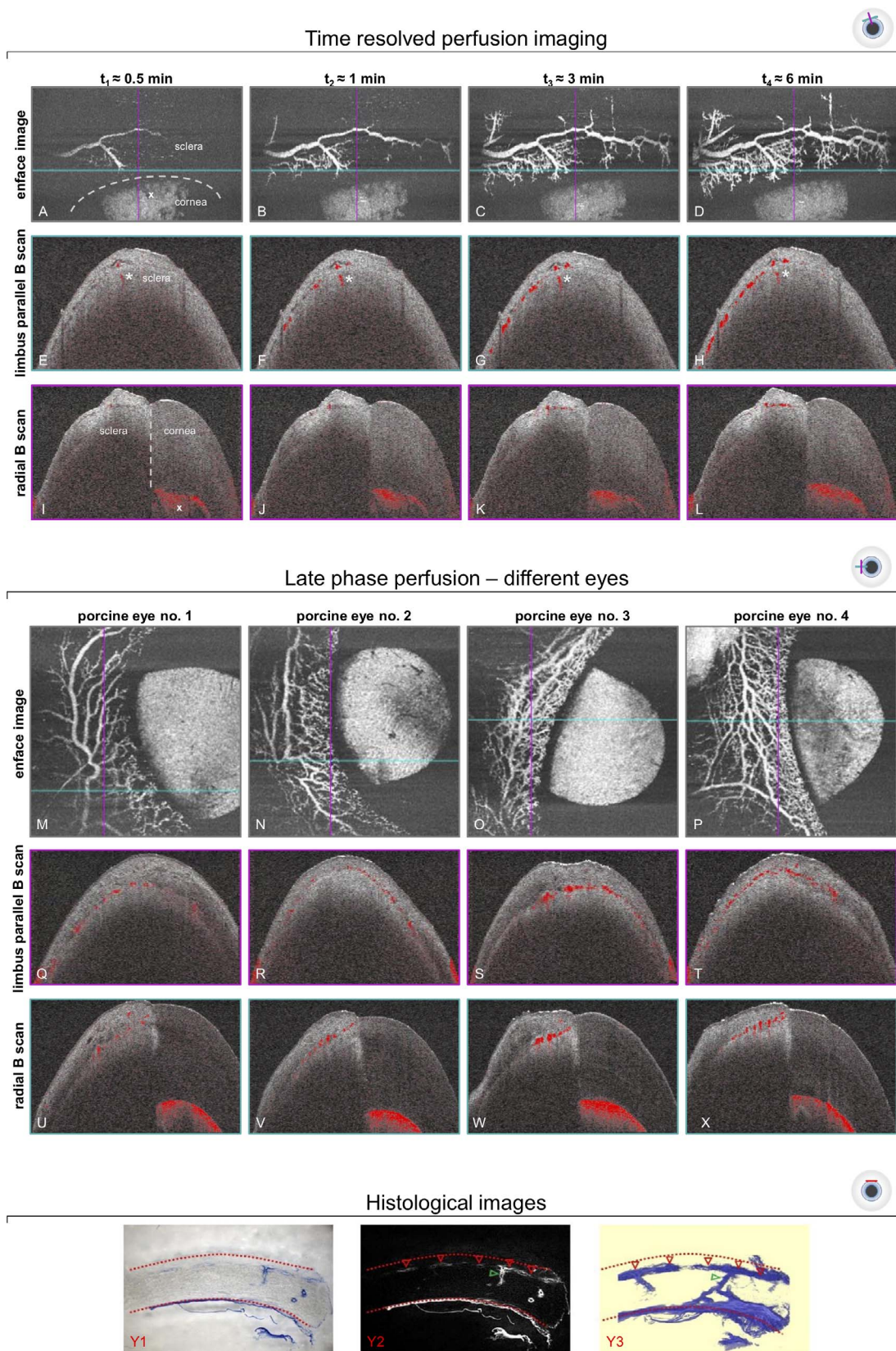
FIGURE 4. Aqueous angiography of ex vivo porcine eyes. (**A–L**) Time-resolved perfusion imaging. In addition to en face images (**A–D**), limbus parallel (**E–H**) and radial (**I–L**) B-scans provide depth information. The *colored lines* in **A–D** indicate the B-scan position. All B-scans show an overlay of the morphologic OCT image (*gray*) and the OCTA signal (*red*). The *asterisk* in **E–H** labels the large diameter aqueous vein, which drains the aqueous from the chamber angle to the superficial vein plexus. The *cross mark* in **I** labels the anterior chamber. (**M–X**) Four different porcine eyes imaged at a late phase of perfusion (5 to 6 minutes). Anatomic variability appeared at the level of the fine juxtalimbal veins with lower (**M**, **N**) or

Investigative Ophthalmology & Visual Science

higher (**O**, **P**) vessel density. (**Y1–Y3**) Limbus parallel histologic sections of an ex vivo porcine eye after perfusion of the aqueous drainage system with Trypan blue. The sections are comparable to OCTA images **E–H** and **Q–T**. The *dotted red lines* label the eye's surface (*top*) and the sclera-chamber angle border. (**Y1**) Unprocessed light microscopy image with the aqueous veins stained *blue*. (**Y2**) Processed image Y1 with extracted Trypan blue signal. The superficial aqueous vein plexus similar to the plexus detected with OCTA in **F–H** and **Q–T** is labeled with *red triangles*. The *green triangle* highlights a large diameter angular aqueous plexus vein similar to the one seen in OCTA (**E–H**, *asterisk*). (**Y3**) 3D rendering of the Trypan blue signal from 23 consecutive kryosections (including **Y2**), representing a tissue volume of approximately 400 μm thickness. The superficial vein plexus and the inner border of the sclera/chamber angle appear blurred due to deformation of the kryosections. This volume demonstrates that the large angular aqueous plexus vein (*green triangle*) originated directly from the chamber angle and that no additional deep aqueous vein plexus was present, which might have been missed with OCTA due to its limited penetration depth.

(approximately 20 μm)[26]; however, the diameter of the smallest juxtalimbal branches of the plexus has not been reported.

The aqueous outflow dynamics observed in this ex vivo study were very different from the human eye. Although in humans the aqueous flow converges from multiple small collector channels and aqueous veins to larger vessels, the porcine eye showed the primary filling of single large diameter veins from which the aqueous was distributed either into episcleral veins or into a fine superficial juxtalimbal aqueous vein plexus without further connection to other draining structures or the anterior chamber. It remains conceivable, however, that occlusion of a preexisting connection to the anterior chamber has occurred postmortem and that, in vivo, some flow exists, potentially depending on the IOP. This remains to be investigated. Another uncertainty is the nature of the juxtalimbal plexus: its superficial position and the fine branching toward the limbus might indicate that it is in fact a plexus of blood vessels, which, in the absence of blood flow, was retrogradely filled with aqueous. This would be in line with the anatomical description of McMenamin and Steptoe.[26] In the histologic sections, no erythrocytes were found in this area, which, however, does not proof the absence of blood. In vivo OCTA imaging might clarify this point but was not feasible during this project.

Recent data from Loewen et al.[7] support our finding that a small number of primary vessels drains the aqueous humor. They observed between one and three distinct drainage sites per eye. McMenamin and Streptoe[26] reported four to eight vessels of the angular aqueous plexus; however, this number was derived from histologic sections and not from cast preparations of the whole vessel system, making it conceivable that the number was overestimated due to bending of the vessels.

The penetration depth of our LE-OCTA setup was approximately half the scleral thickness near the limbus. More posteriorly, it was further reduced if the tenon tissue overlying the sclera was very swollen. Therefore, the aqueous veins of the angular aqueous plexus (Figs. 4E–4H, asterisk, 5E, 5F) could not be imaged down to their origin in the chamber angle. However, the data from the ICG/SLO imaging and the Trypan blue/histologic sections confirmed that no additional aqueous vein plexus existed, which we might have missed with LE/OCTA imaging. In the future, the use of longer wavelength OCTA, such as newly available SS devices, would further increase the penetration depth, presumably allowing full scleral thickness imaging.

Aqueous solutions, such as ICG and fluorescein, have been previously used for in vivo and ex vivo aqueous angiography.[6,27–29] Recent advances in fluorescence detection and image processing have improved both spatial and temporal
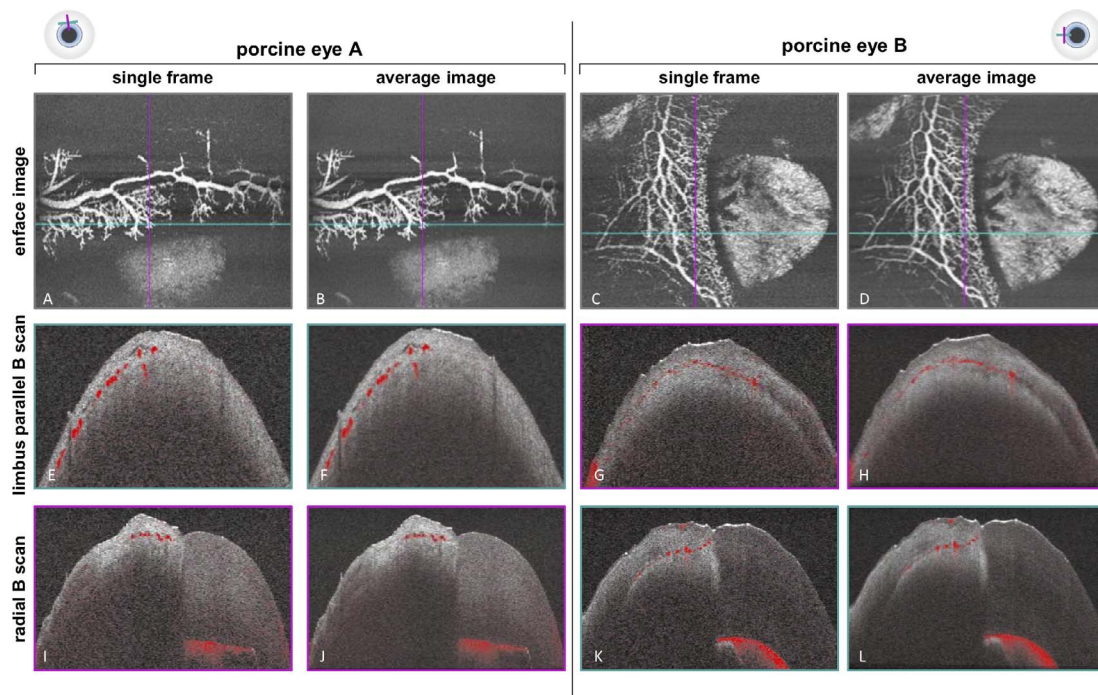

FIGURE 5. The effect of averaging multiple OCTA images on image quality. Of two porcine eyes, single OCTA images (**A**, **E**, **I** and **C**, **G**, **K**) were compared with the average of four consecutively acquired OCTA images (**B**, **F**, **J** and **D**, **H**, **L**). Averaging of this relatively small number of images led to improved signal-to-noise ratio.

resolution and quantification of the aqueous flow signal.[7,30] A major advantage of an OCTA-based technology, however, is that it provides 3D data, whereas a major disadvantage is that the temporal resolution is low due to the large datasets that need to be acquired and processed. Data oversampling for averaging images at each time point further impairs temporal resolution to a point where dynamic changes in perfusion cannot be resolved. However, the application of faster OCT scanners, such as SS-OCT, the use of faster computer hardware, and the development of OCTA-averaging algorithms would certainly improve the temporal resolution of time-resolved OCTA sequences. Furthermore, the longer wavelengths utilized in modern SS-OCT might render this technology superior to ICG-based SLO imaging regarding penetration depth.

From a clinical point of view, aqueous angiography, despite being known for decades, has never established as a routine diagnostic tool in glaucoma surgery. We believe, however, that a number of recently emerged factors could promote its application in the future: (1) glaucoma surgical techniques opening or bypassing the trabecular meshwork such as Trabectome, Kahook dual blade, Goniotome, and iStent have established, among others, as standard procedures in open angle glaucoma surgery, and (2) recent experimental ex vivo data suggest that using aqueous angiography prior to iStent implantation allows one to specifically implant the stent in low flow areas. By doing this, a significant increase in flow was detected in this particular segment.[31] Thus, aqueous angiography might help to target stents or goniotomy procedures to areas where an increase in flow is highly likely. (3) Intraoperative imaging technology, mainly intraoperative OCT, is an emerging technology, augmenting the information gained through the surgical microscope. We expect intraoperative OCT to become a widespread technology in the ophthalmology operating theater of the future. Given the rapid technological development, this will likely include OCTA. Thus, an imaging technology to detect LE as contrast agents would be readily available.

According to a recent proof-of-concept publication, the intracameral application of ICG appeared to be safe in human eyes in vivo.[32] For LEs, this point remains to be investigated, particularly the interaction of lipid micelles with the trabecular meshwork requires further research before application in humans.

References

1. Ashton N. Anatomical study of Schlemm's canal and aqueous veins by means of neoprene casts. Part I. Aqueous veins. *Br J Ophthalmol*. 1951;35:291–303.

2. Ashton N. Anatomical study of Schlemm's canal and aqueous veins by means of neoprene casts. II. Aqueous veins. *Br J Ophthalmol*. 1952;36:265–267.

3. Kagemann L, Wollstein G, Ishikawa H, et al. Visualization of the conventional outflow pathway in the living human eye. *Ophthalmology*. 2012;119:1563–1568.

4. Uji A, Muraoka Y, Yoshimura N. In vivo identification of the posttrabecular aqueous outflow pathway using swept-source optical coherence tomography. *Invest Opthalmol Vis Sci*. 2016;57:4162–4169.

5. Fellman RL, Feuer WJ, Grover DS. Episcleral venous fluid wave correlates with trabectome outcomes: intraoperative evaluation of the trabecular outflow pathway. *Ophthalmology*. 2015;122:2385–2391.

6. Grieshaber MC, Pienaar A, Olivier J, Stegmann R. Clinical evaluation of the aqueous outflow system in primary open-angle glaucoma for canaloplasty. *Invest Ophthalmol Vis Sci*. 2010;51:1498–1504.

7. Loewen RT, Brown EN, Roy P, Schuman JS, Sigal IA, Loewen NA. Regionally discrete aqueous humor outflow quantification using fluorescein canalograms. *PLoS One*. 2016;11:e0151754.

8. Saraswathy S, Tan JCH, Yu F, et al. Aqueous angiography: real-time and physiologic aqueous humor outflow imaging. *PLoS One*. 2016;11:e0147176.

9. Huang D, Swanson EA, Lin CP, et al. Optical coherence tomography. *Science*. 1991;254:1178–1181.

10. Drexler W, Liu M, Kumar A, Kamali T, Unterhuber A, Leitgeb RA. Optical coherence tomography today: speed, contrast, and multimodality. *J Biomed Opt*. 2014;19:071412.

11. de Boer JF, Cense B, Park BH, Pierce MC, Tearney GJ, Bouma BE. Improved signal-to-noise ratio in spectral-domain compared with time-domain optical coherence tomography. *Opt Lett*. 2003;28:2067–2069.

12. Chinn SR, Swanson EA, Fujimoto JG. Optical coherence tomography using a frequency-tunable optical source. *Opt Lett*. 1997;22:340–342.

13. Choma MA, Hsu K, Izatt JA. Swept source optical coherence tomography using an all-fiber 1300-nm ring laser source. *J Biomed Opt*. 2005;10:44009.

14. Zhang A, Zhang Q, Chen C-L, Wang RK. Methods and algorithms for optical coherence tomography-based angiography: a review and comparison. *J Biomed Opt*. 2015;20:100901.

15. Gao SS, Jia Y, Zhang M, et al. Optical coherence tomography angiography. *Invest Opthalmol Vis Sci*. 2016;57:OCT27–OCT36.

16. Wang B, Kagemann L, Schuman JS, et al. Gold nanorods as a contrast agent for Doppler optical coherence tomography. *PLoS One*. 2014;9:e90690.

17. de la Zerda A, Prabhulkar S, Perez VL, et al. Optical coherence contrast imaging using gold nanorods in living mice eyes. *Clin Exp Ophthalmol*. 2015;43:358–366.

18. Prabhulkar S, Matthews J, Rawal S, Awdeh RM. Molecular histopathology using gold nanorods and optical coherence tomography. *Invest Ophthalmol Vis Sci*. 2013;54:1192–1200.

19. Alkilany AM, Shatanawi A, Kurtz T, Caldwell RB, Caldwell RW. Toxicity and cellular uptake of gold nanorods in vascular endothelium and smooth muscles of isolated rat blood vessel: importance of surface modification. *Small*. 2012;8:1270–1278.

20. Wan J, Wang J-H, Liu T, Xie Z, Yu X-F, Li W. Surface chemistry but not aspect ratio mediates the biological toxicity of gold nanorods in vitro and in vivo. *Sci Rep*. 2015;5:11398.

21. Napoli PE, Coronella F, Satta GM, Fossarello M. A novel technique of contrast-enhanced optical coherence tomography imaging in evaluation of clearance of lipids in human tears. *PLoS One*. 2014;9:e109843.

22. Pan Y, You J, Volkow ND, Park K, Du C. Ultrasensitive detection of 3D cerebral microvascular network dynamics in vivo. *NeuroImage*. 2014;103:492–501.

Investigative Ophthalmology & Visual Science

23. Schindelin J, Arganda-Carreras I, Frise E, et al. Fiji: an open-source platform for biological-image analysis. *Nat Methods*. 2012;9:676–682.

24. Schuck P. Size-distribution analysis of macromolecules by sedimentation velocity ultracentrifugation and lamm equation modeling. *Biophys J*. 2000;78:1606–1619.

25. Ruiz-Ederra J, García M, Hernández M, et al. The pig eye as a novel model of glaucoma. *Exp Eye Res*. 2005;81:561–569.

26. McMenamin PG, Steptoe RJ. Normal anatomy of the aqueous humour outflow system in the domestic pig eye. *J Anat*. 1991; 178:65–77.

27. Wessely K. Die physiologischen und anatomischen Grundlagen der neueren Glaukomoperationen [in German]. *Verslg Ophthalm Ges Heidelb*. 1922;35–100.

28. Benedikt O. Demonstration of aqueous outflow patterns of normal and glaucomatous human eyes through the injection of fluorescein solution in the anterior chamber (author's transl). *Albrecht Von Graefes Arch Für Klin Exp Ophthalmol*. 1976;199:45–67.

29. Grote P. Indications for the location of trabeculotomy in simple glaucoma. II. The demonstration of aqueous outflow with fluorescein [in German]. *Doc Ophthalmol Adv Ophthalmol*. 1978;46:171–183.

30. Saraswathy S, Tan JCH, Yu F, et al. Aqueous angiography: real-time and physiologic aqueous humor outflow imaging. *PLoS One*. 2016;11:e0147176.

31. Huang AS, Saraswathy S, Dastiridou A, et al. Aqueous angiography-mediated guidance of trabecular bypass improves angiographic outflow in human enucleated eyes. *Invest Ophthalmol Vis Sci*. 2016;57:4558–4565.

32. Huang AS, Camp A, Xu BY, Penteado RC, Weinreb RN. Aqueous angiography: aqueous humor outflow imaging in live human subjects. *Ophthalmology*. 2017;124:1249–1251.